Evolution of a Bose-Einstein condensate in a rapidly expanding circular box

Stavros Theodorakis* and Yiannis Constantinou
Physics Department, University of Cyprus, P.O. Box 20537, Nicosia 1678, Cyprus
(Received 29 April 2007; revised manuscript received 25 June 2007; published 12 September 2007)

We examine the evolution of the ground state of a Bose-Einstein condensate in a two-dimensional circular box, the wall of which is initially at rest and then recedes with large and constant speed. The final state of the condensate depends on the rapidity of the expansion of the box. If the number of atoms in the condensate is small compared to the dimensionless speed of the wall, then the condensate becomes a mixture of excitations and follows the expansion of the box, leaving empty though an increasingly larger region between the condensate boundary and the wall. If, on the other hand, the number of atoms is large compared to the dimensionless speed of the wall, then the condensate is always in the ground state and spreads uniformly in all of the expanding box, the condensate boundary always coinciding with the receding wall. Approximate analytic expressions are found for the evolving wave function.

DOI: 10.1103/PhysRevE.76.036205 PACS number(s): 05.45.−a, 03.75.−b, 03.65.Ge

I. INTRODUCTION

The recent production of Bose-Einstein condensates in box traps [1] has created an increased interest in nonlinear systems confined in such traps, leading, for example, to the study of the influence of a periodic driving force on these systems [2]. One-dimensional box traps have attracted interest quite early, because they result in analytic solutions for the wave functions of the Bose-Einstein condensates [3]. The evolution of the condensates if the box trap is time varying is particularly interesting as well, since its study may elucidate the interplay between the nonlinearity and the dynamics. This interplay has already been studied for the case of a particular one-dimensional box, the size of which is first doubled and then halved [4]. These studies are rendered difficult though by the fact that the nonlinearities have to be treated numerically in most of the cases, the time dependence of the boundaries of the box further complicating the matter.

This work will examine the evolution of the ground state of a Bose-Einstein condensate with repulsive interactions in a rapidly expanding two-dimensional circular box, the wall of which begins at rest and ends up having a large constant speed. This particular configuration presents the advantage of having approximate analytic solutions in closed form. Even though one would naively expect that the adiabatic approximation does not hold for such a rapidly expanding box, higher excitations being necessarily involved in the evolution of the initial ground state, we find that this is not so when the nonlinearities are sufficiently strong. Indeed, if the repulsive two-body interactions are very strong, the wave function will be forced to occupy all the available area, spreading therefore uniformly over the rapidly expanding box and adopting the profile of the ground state. In contrast, if the nonlinearity is weak and the wall is moving rapidly, the wave function adopts the profile that is appropriate to the sudden approximation. Thus the problem becomes similar then to the well-known linear problem of a quantum particle in a box with moving walls [5].

*stavrost@ucy.ac.cy

Let us begin with the Gross-Pitaevskii (GP) equation, which describes the evolution of a Bose-Einstein condensate confined in a two-dimensional box:

$$-\frac{\hbar^2}{2m}\nabla^2\Psi + g|\Psi|^2\Psi = i\hbar\frac{\partial\Psi}{\partial t}, \tag{1}$$

where g is positive (repulsive two-body interactions), $0 \leqslant |\vec{r}| \leqslant L(t)$, and Ψ is zero when $|\vec{r}| \geqslant L(t)$. The condensate is confined thus in a circular box with radius $L(t)$. We expect, of course, its ground state to be radially symmetric.

This equation is rather difficult to solve if $L(t)$ is arbitrary. The corresponding linear problem has analytic solutions though for the particular case that $L(t)^3 d^2L/dt^2$ is constant [6]. We shall examine thus in this work the particular case $L(t)=L_0\sqrt{1+(t/T)^2}$ for times $t \geqslant 0$ and $L(t)=L_0$ for times $t \leqslant 0$. The wall of the box is motionless for $t \leqslant 0$ and ends up moving finally with a terminal speed L_0/T.

We define the dimensionless variables $x=|\vec{r}|/L_0$, $\tau = \hbar t/(2mL_0^2)$, $l(t)=L(t)/L_0$, and $\phi(x,\tau) = \Psi(\vec{r},t)\sqrt{2mgL_0^2/\hbar^2}/\Psi_0$, where the dimensionless parameter Ψ_0 is $\Psi_0=\Psi(0,0)\sqrt{2mgL_0^2/\hbar^2}$. Thus $\phi(0,0)=1$ and $0 \leqslant x \leqslant l(t)$. The number of atoms in the condensate is $N = \int|\Psi|^2 d^2r = \hbar^2\Psi_0^2(2mg)^{-1}\int_0^{l(t)} 2\pi x|\phi(x,\tau)|^2 dx$. We note that in this work $l(t)=\sqrt{1+\nu^2\tau^2}$ if $t \geqslant 0$ and $l(t)=1$ if $t \leqslant 0$, where ν is the dimensionless parameter $\nu = 2mL_0^2/(\hbar T)$.

The GP equation takes thus the dimensionless form

$$-\nabla_x^2\phi + \Psi_0^2|\phi|^2\phi = i\frac{\partial\phi}{\partial\tau}, \tag{2}$$

where $\phi(0,0)=1$, $\phi(l(\tau),\tau)=0$. It is this nonlinear partial differential equation that will determine the condensate wave function.

II. NEGATIVE TIMES

Let us first solve this equation for times $t \leqslant 0$. We shall assume that the condensate is initially in its ground state, with $\phi(1,\tau)=0$ and $\phi(0,0)=1$. Since the condensate is in a

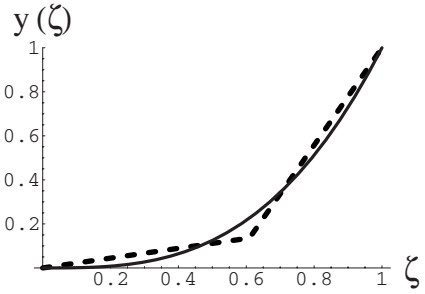

FIG. 1. The curve $y(\zeta)=\zeta^3$ and its piecewise linear emulator $f(\zeta)$. The solid curve is the line ζ^3, while the dashed one is the emulator.

stationary state, we shall have $\phi(x,\tau)=e^{-i\beta\tau}\zeta(x)$, with $\zeta(0)=1$ and $\zeta(1)=0$. Thus the GP equation reduces to

$$-\frac{d^2\zeta}{dx^2}-\frac{1}{x}\frac{d\zeta}{dx}+\Psi_0^2\zeta^3=\beta\zeta. \tag{3}$$

This equation cannot be solved analytically due to the ζ'/x term, unlike the one-dimensional case [3]. We note, however, that $\zeta\approx 1$ and $\beta\approx\Psi_0^2$ when the number of atoms is large enough, since the condensate is then uniform almost everywhere. For large β we expect thus that the derivatives in the GP equation can be safely neglected almost everywhere.

Nonetheless, we can obtain an excellent analytic approximation for the ground state $\zeta(x)$ for any value of β if we emulate the curve $\zeta^3(x)$ by a piecewise linear function of ζ [7]. In other words, we shall replace the nonlinearity ζ^3 with an appropriate piecewise linear emulator function $f(\zeta)$, such that the integral $\int_0^1[\zeta^3-f(\zeta)]^2d\zeta$ is minimized. If this emulator function is a reasonable approximation to the curve ζ^3, then good approximate analytic solutions of the GP equation can be obtained by solving the linear partial differential equations that result when ζ^3 is replaced by $f(\zeta)$.

Let us adopt then the function

$$\begin{aligned} f(\zeta)&=a\zeta+b \quad \text{if } \zeta_0\leqslant\zeta\leqslant 1\\ f(\zeta)&=c\zeta \quad \text{if } 0\leqslant\zeta\leqslant\zeta_0, \end{aligned} \tag{4}$$

requiring that the end points of the continuous function $f(\zeta)$ coincide with the end points of ζ^3. Hence $a=(1-c\zeta_0)/(1-\zeta_0)$ and $b=(c-1)\zeta_0/(1-\zeta_0)$. We require furthermore that the two curves be as close as possible. We can achieve this by minimizing the integral of the square of the difference between the emulated curve ζ^3 and its emulator $f(\zeta)$. We obtain $a=(48+13\sqrt{2})/30=2.212\,83$, $b=1-a=(-18-13\sqrt{2})/30=-1.212\,83$, $c=(9-4\sqrt{2})/15=0.222\,876$, and $\zeta_0=(2\sqrt{2}-1)/3=0.609\,476$. The corresponding function $f(\zeta)$ is then indeed quite close to the function $y(\zeta)=\zeta^3$, as can be seen in Fig. 1.

After emulation the GP equation reduces to

$$-\frac{d^2\zeta}{dx^2}-\frac{1}{x}\frac{d\zeta}{dx}+\Psi_0^2(a\zeta+b)=\beta\zeta \tag{5}$$

if $\zeta_0\leqslant\zeta\leqslant 1$ and

$$-\frac{d^2\zeta}{dx^2}-\frac{1}{x}\frac{d\zeta}{dx}+c\Psi_0^2\zeta=\beta\zeta \tag{6}$$

if $0\leqslant\zeta\leqslant\zeta_0$. Since the wave function of the ground state is monotonically decreasing, the solution $\zeta_{in}(x)$ of Eq. (5) will hold for $0\leqslant x\leqslant x_0$, where $\zeta(x_0)=\zeta_0$, while the solution $\zeta_{out}(x)$ of Eq. (6) will hold for $x_0\leqslant x\leqslant 1$.

We can easily solve these two equations, obtaining the solutions in terms of simple Bessel functions. In the region $0\leqslant x\leqslant x_0$ $\zeta(x)=\zeta_{in}(x)$,

$$\zeta_{in}(x)=I_0(qx)+\frac{\zeta_0-I_0(qx_0)}{I_0(qx_0)-1}[I_0(qx)-1], \tag{7}$$

with $q=\sqrt{a\Psi_0^2-\beta}$ and

$$I_0(qx_0)=(q^2\zeta_0+b\Psi_0^2)/(q^2+b\Psi_0^2). \tag{8}$$

We note that $\zeta_{in}(0)=1$ and $\zeta_{in}(x_0)=\zeta_0$. For large nonlinearities Ψ_0, we expect $\zeta_{in}(x)$ to be practically uniform and to extend almost up to the wall $x=1$. Hence, in that limit, $\Psi_0^2\approx\beta$, rendering $I_0(qx_0)$ large and hence the denominator $q^2+b\Psi_0^2$ very small, $q^2+b\Psi_0^2\approx 0$. Thus

$$q\approx\sqrt{-b\beta}. \tag{9}$$

The condition $I_0(qx_0)=(q^2\zeta_0+b\Psi_0^2)/(q^2+b\Psi_0^2)$ reduces then to

$$\Psi_0^2\approx\beta-b\beta(\zeta_0-1)/I_0(qx_0). \tag{10}$$

In the region $x_0\leqslant x\leqslant 1$, $\zeta(x)=\zeta_{out}(x)$,

$$\zeta_{out}(x)=\zeta_0\frac{J_0(kx)Y_0(k)-J_0(k)Y_0(kx)}{J_0(kx_0)Y_0(k)-J_0(k)Y_0(kx_0)}, \tag{11}$$

where $k=\sqrt{\beta-c\Psi_0^2}$. We note that $\zeta_{out}(x_0)=\zeta_0$ and $\zeta_{in}(1)=0$.

Then continuity of $\zeta'(x)$ at x_0 requires that

$$\frac{qI_1(qx_0)(\zeta_0-1)}{k\zeta_0[I_0(qx_0)-1]}=\frac{J_0(k)Y_1(kx_0)-J_1(kx_0)Y_0(k)}{J_0(kx_0)Y_0(k)-J_0(k)Y_0(kx_0)}. \tag{12}$$

The parameters x_0 and Ψ_0 are determined by the simultaneous solution of Eqs. (8) and (12). The resulting analytic closed-form expressions for the wave function for $t\leqslant 0$ provide very good simulacra to the numerically obtained wave functions for all values of β, as shown in Fig. 2 for the particular choice of $\beta=64$ and $\Psi_0=7.9982$. The numerical solution was obtained by using the explicit Runge-Kutta method, the value of Ψ_0 having been found iteratively so as to satisfy $\zeta(1)=0$.

For large Ψ_0, in which case $\Psi_0^2\approx\beta$ and $k\approx\sqrt{\beta(1-c)}$, Eq. (12) yields

$$\begin{aligned} x_0&\approx 1-\frac{1}{\sqrt{\beta(1-c)}}\tan^{-1}[\zeta_0\sqrt{(c-1)/b}/(1-\zeta_0)]\\ &\approx 1-1.016133/\sqrt{\beta}, \end{aligned} \tag{13}$$

while Eq. (10) becomes

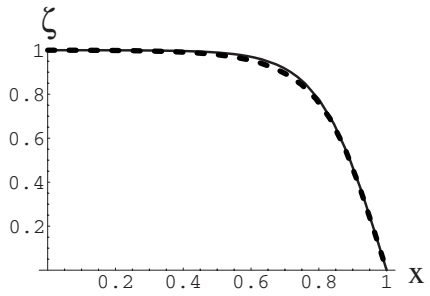

FIG. 2. The wave function $\zeta(x)$ for $\beta=64$, $\Psi_0=7.9982$ and negative times. The solid curve is the numerical solution, while the dashed one is its analytic simulacrum.

$$\Psi_0^2 \approx \beta - 3.814903\beta^{5/4}e^{-\sqrt{-b\beta}}. \tag{14}$$

This asymptotic expression is fairly accurate, as can be seen in Fig. 3, where it is compared with the numerically determined Ψ_0.

III. POSITIVE TIMES

The solution given by Eqs. (7) and (11) gives the wave function at time $t \leqslant 0$. The circular box begins expanding though at time $t=0$, its radius being $l(\tau)=\sqrt{1+\nu^2\tau^2}$, so that $l(\tau)^3 d^2 l(\tau)/d\tau^2=\nu^2$. Note that $l(0)=1$ and $dl(0)/d\tau=0$. The solution of Eq. (2) is going to give the wave function for positive times.

This solution can be obtained through a pseudoconformal transformation [8] that has been used for the corresponding linear problem [9]. Indeed, let us define the new variables

$$x' = x/l(\tau) \tag{15}$$

and

$$\tau' = \nu^{-1}\tan^{-1}(\nu\tau), \tag{16}$$

so that $d\tau'/d\tau=1/l(\tau)^2$. We note that $0 \leqslant \tau' \leqslant \frac{\pi}{2\nu}$. We shall also define a new wave function $\vartheta(x',\tau')$ through the equation

$$\phi(x,\tau) = l(\tau)^{-1}\vartheta(x',\tau')e^{i\gamma(\tau)x^2}, \tag{17}$$

where

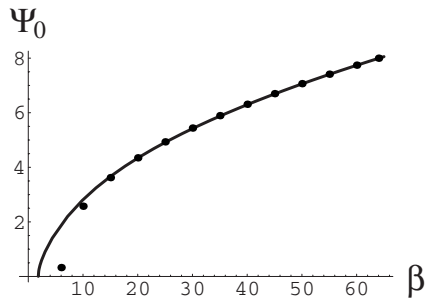

FIG. 3. The value of Ψ_0, given by Eq. (14), compared to the Ψ_0 deduced numerically. The solid curve corresponds to the asymptotic expression, while the points correspond to the numerically obtained values.

$$\gamma(\tau) = \frac{1}{4l(\tau)}\frac{dl(\tau)}{d\tau} = \frac{\nu^2\tau}{4l^2(\tau)}. \tag{18}$$

The new wave function $\vartheta(x',\tau')$ must satisfy the initial condition $\vartheta(x',0)=\phi(x,0)=\zeta(x)$, hence $\vartheta(0,0)=\zeta(0)=1$, as well as the boundary condition $\vartheta(1,\tau')=0$. In terms of the new variables Eq. (2) takes the form

$$-\frac{d^2\vartheta}{dx'^2} - \frac{1}{x'}\frac{d\vartheta}{dx'} + \Psi_0^2|\vartheta|^2\vartheta + \frac{\nu^2 x'^2}{4}\vartheta = i\frac{\partial\vartheta}{\partial\tau'}. \tag{19}$$

We note that the coefficient of the cubic term is time independent. This is not the case if the dimension of the system is equal to 1 [8], leading thus to a qualitatively different behavior for the rapidly expanding one-dimensional box.

If we define the new variable $y=\sqrt{\nu}x'$, then Eq. (19) reduces to

$$-\frac{d^2\vartheta}{dy^2} - \frac{1}{y}\frac{d\vartheta}{dy} + \frac{\Psi_0^2}{\nu}|\vartheta|^2\vartheta + \frac{y^2}{4}\vartheta = \frac{i}{\nu}\frac{\partial\vartheta}{\partial\tau'}, \tag{20}$$

subject to the conditions $\vartheta(0,0)=1$ and $\vartheta(\sqrt{\nu},\tau')=0$. So for large ν the wave function ϑ tends to zero far from the origin.

A. Linear limit ($\Psi_0^2 \ll \nu$)

If $\Psi_0^2 \ll \nu$, then Eq. (20) takes the approximate form

$$-\frac{d^2\vartheta}{dy^2} - \frac{1}{y}\frac{d\vartheta}{dy} + \frac{y^2}{4}\vartheta = i\frac{\partial\vartheta}{\partial(\nu\tau')}, \tag{21}$$

with ϑ tending to 0 far from the origin when ν is large.

In other words, if we perform the pseudoconformal transformation mentioned above on the rapidly expanding box, then we end up with Eq. (21), an equation describing the radially symmetric modes of the usual two-dimensional simple harmonic oscillator. The general solution of this equation is the superposition of these modes, expressed in terms of Laguerre polynomials:

$$\vartheta(x',\tau') \approx \sum_n c_n e^{-i(2n+1)\nu\tau'}L_n(\nu x'^2/2)e^{-\nu x'^2/4}. \tag{22}$$

Since $\vartheta(x',0)=\zeta(x')$, where $\zeta(0)=1$ and $\zeta(1)=0$, we can find the coefficients c_n:

$$c_n \approx \int_0^1 \zeta(x')\nu x' L_n(\nu x'^2/2)e^{-\nu x'^2/4}dx'. \tag{23}$$

Even though the various radially symmetric modes vanish far away from the origin, the coefficients c_n are such that the superposition of these modes in Eq. (22) at time 0 yields $\zeta(x')$, a function spreading almost uniformly over all of the box. As time progresses though and $\tau \to \infty$, the transformed time τ' tends to $\pi/(2\nu)$. Hence

$$\vartheta \to -i\sum_n (-1)^n c_n L_n(\nu x'^2/2)e^{-\nu x'^2/4}. \tag{24}$$

Thus the profile of ϑ is stabilized as $\tau \to \infty$. The coefficients c_n alternate in sign now in the superposition, so ϑ

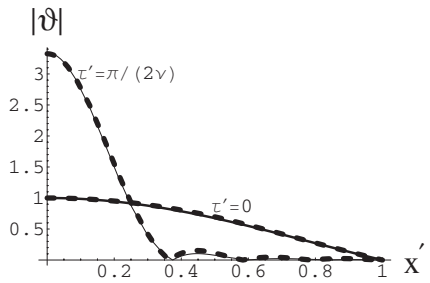

FIG. 4. The wave function $|\vartheta(x',\tau')|$ for $\beta=6$, $\Psi_0=0.617$, and $\nu=30$ for times $\tau'=0$ and $\tau'=\pi/(2\nu)$. The solid curves correspond to the numerical solutions of Eq. (19), while the dashed curves correspond to the analytic expressions of Eq. (22).

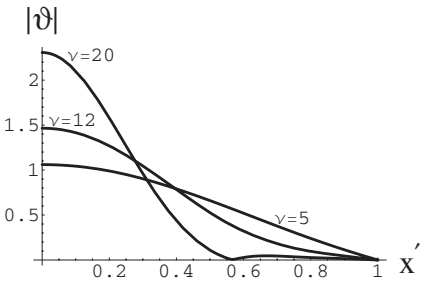

FIG. 5. The numerical solutions of Eq. (19) for the wave function $|\vartheta(x',\tau')|$, for $\beta=5.78319$ and $\Psi_0=0$ at times $t=\pi/(2\nu)$, when ν takes the values 5, 12, 20.

cannot extend all the way up to the wall, given the localized nature of the radially symmetric modes. We expect thus the wave function ϑ of Eq. (22) to freeze in a region around the origin, leaving a void in the remaining area up to the wall, as seen in Fig. 4 for the case $\beta=6$ and $\nu=30$.

The radius of the area where the condensate has been concentrated is of the order of the width of the Gaussian $e^{-\nu x'^2/4}$ that appears in Eq. (24)—i.e., $x'\approx 2/\sqrt{\nu}$ or $x\approx 2l(\tau)/\sqrt{\nu}$. In other words, as time progresses the radius of the condensate increases at an approximately constant rate of the order of $2\sqrt{\nu}$, while the wall is receding with speed ν. The increasing concentration of the condensate is the result of the destructive interference that takes place between the various radially symmetric modes of the two-dimensional simple harmonic oscillator to which the problem has been reduced.

What essentially happens in this linear region at $t=0$ is that the eigenstate basis changes at that instant. Before $t=0$ the energy eigenstates are the states of a particle in a circular box. After $t=0$ the energy eigenstates are the states of an isotropic two-dimensional harmonic oscillator. As a result of this abrupt change of basis, the initial ground state of the stationary box suddenly becomes a superposition of oscillator states [10]. The interference between these states at various moments in time, already explored in detail in the context of the linear Schrödinger equation for a particle in a box with a moving wall [5,11], is responsible for the restriction of the condensate to a small region in the center of the expanding box.

Thus, even though Ψ_0^2 may be large, the condensate is in the linear limit if $\nu \gg \Psi_0^2$. Indeed, larger values of ν at a particular moment in time imply that the condensate is more dilute, as it should be in the linear limit. Conversely, smaller values of Ψ_0^2 imply a smaller number of atoms—i.e., a more dilute condensate again. Thus we can reach the linear regime either by decreasing Ψ_0^2 or by increasing ν, or both. The linearity or nonlinearity of the system emerges consequently from the comparison of the quantities Ψ_0^2 and ν, just as is the comparison of the various time scales that determines whether the dynamics is adiabatic for a Bose-Einstein condensate in a time-dependent potential [12].

Let us illustrate the above results by solving the linear limit ($\Psi_0=0$) of Eq. (19) numerically, given the initial condition $\vartheta(x',0)=\zeta(x')$, where ζ is found by solving Eq. (3) numerically. There exist solutions that always extend over the whole area of the box (adiabatic behavior, $\nu \ll 12$), as well as solutions that retreat towards the center of the box as time goes on (sudden approximation, $\nu \gg 12$). In Fig. 5 such numerical solutions are shown for $\nu=5$, $\nu=12$, and $\nu=20$, at times $t=\pi/(2\nu)$, for the case $\beta=5.783\,19$ and $\Psi_0=0$. Thus "large ν" must be taken to mean $\nu>12$, since only then will the linear problem ($\Psi_0=0$) have its solutions localized near the center.

B. Nonlinear limit ($\Psi_0^2 \gg \nu$)

Let us now examine what is expected to happen when $\Psi_0^2 \gg \nu$. We begin by finding the profile of the stationary ground state of Eq. (19), assuming thus that $\vartheta(x',\tau')=\theta(x')e^{-i\delta\tau'}$, with $\theta(0)=1$ and $\theta(1)=0$. The resulting equation

$$-\frac{d^2\theta}{dx'^2}-\frac{1}{x'}\frac{d\theta}{dx'}+\frac{\nu^2 x'^2}{4}\theta+\Psi_0^2\theta^3=\delta\theta \tag{25}$$

yields the stationary ground state of Eq. (19).

If $\Psi_0^2 \gg \nu$, we expect the ground-state condensate to be quite dense and to spread out uniformly over the box. In other words, the derivatives in Eq. (25) may be neglected. Then this equation yields the Thomas-Fermi approximation

$$\theta^2 \approx \left(\delta-\frac{\nu^2 x'^2}{4}\right)/\Psi_0^2. \tag{26}$$

Since $\vartheta(0,0)=1$, we must have $\delta\approx\Psi_0^2$. Hence

$$\vartheta(x',\tau') \approx \sqrt{1-\frac{\nu^2 x'^2}{4\Psi_0^2}}e^{-i\Psi_0^2\tau'}. \tag{27}$$

Equation (27) indicates that the boundary of the dense condensate is at $x'\approx 2\Psi_0/\nu$. However, the boundary of the box is at $x'=1$.

Thus, if $1<2\Psi_0/\nu$, the natural extent of the condensate is larger than the size of the box. Hence the circular wall will cut off abruptly the profile of the condensate, which will therefore remain uniform over all of the box, going abruptly to zero at $x'=1$ and resulting in a negative curvature right up to the wall, as shown in Fig. 6 for $\delta=400$, $\Psi_0=19.971\,65$, $\nu=30$, and $2\Psi_0/\nu=1.33$.

On the other hand, if we had $1>2\Psi_0/\nu$, then the natural extent of the condensate would be smaller than the size of

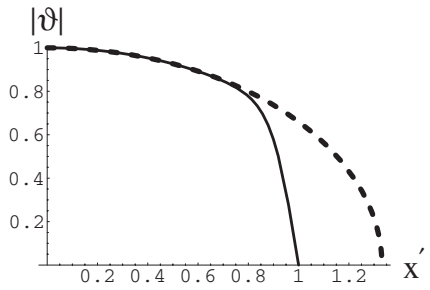

FIG. 6. The solid curve corresponds to the numerically obtained ground state of Eq. (25) for $\delta=400$, $\Psi_0=19.97165$, $\nu=30$, and $2\Psi_0/\nu=1.33$, while the dashed curve corresponds to the Thomas-Fermi approximation of Eq. (27).

the box. Hence the condensate would have ample space for relaxing gradually to zero with positive curvature, long before having to meet the circular wall at $x'=1$, as shown in Fig. 7 for $\delta=64$, $\Psi_0=7.294\,653\,3$, $\nu=30$, and $2\Psi_0/\nu=0.486$.

We see then that the stationary ground state falls to zero with negative curvature if $\nu<2\Psi_0$, the condensate spreading out uniformly up to the wall, and with positive curvature if $\nu>2\Psi_0$, leaving in that case an empty space between the boundary of the condensate and the receding wall.

This feature can be seen most clearly in Fig. 8, where we plot the location of the inflection point of $\theta(x')$, found numerically as a function of $2\Psi_0/\nu$ for the particular choice of $\nu=20$. We see that as $2\Psi_0/\nu$ increases, the inflection point moves quickly towards the wall, where it settles down. Thus the curvature is negative everywhere for large $2\Psi_0/\nu$, except for a tiny interval right on the wall, where the inflection point has settled.

We shall now try to find the solution $\vartheta(x',\tau')$ of Eq. (19) in the nonlinear region, subject not only to the initial condition $\vartheta(x',0)=\zeta(x')$, since $x=x'$ at $\tau=\tau'=0$, but also to the boundary condition $\vartheta(1,\tau')=0$. The initial profile $\zeta(x')$, with $\zeta(0)=1$ and $\zeta(1)=0$, satisfies Eq. (3).

If the initial profile is the stationary ground state of Eq. (19), then the matter will be simple enough, since the solution will be the initial profile multiplied by an evolution phase factor. Otherwise, the solution will necessarily involve higher excitations and the solution will be analytically intrac-

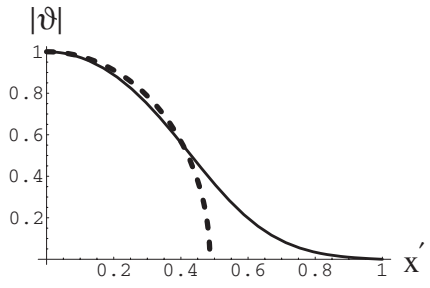

FIG. 7. The solid curve corresponds to the numerically obtained ground state of Eq. (25) for $\delta=64$, $\Psi_0=7.2946533$, $\nu=30$, and $2\Psi_0/\nu=0.486$, while the dashed curve corresponds to the Thomas-Fermi approximation of Eq. (27).

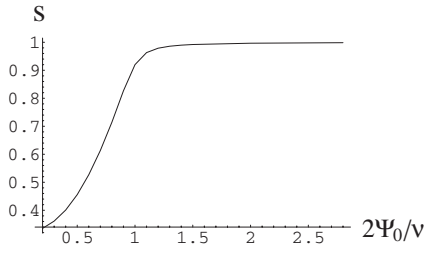

FIG. 8. The location of the inflection point s of the $\theta(x')$ of Eq. (25) as a function of $2\Psi_0/\nu$ for $\nu=20$.

table. Let us assume then that $\vartheta(x',\tau')=\zeta(x')e^{-i\delta\tau'}$. Then Eq. (19) reduces to

$$-\frac{d^2\zeta}{dx'^2}-\frac{1}{x'}\frac{d\zeta}{dx'}+\frac{\nu^2x'^2}{4}\zeta+\Psi_0^2\zeta^3=\delta\zeta. \tag{28}$$

If we combine, however, this equation with Eq. (3), we obtain the relation $\beta+(\nu^2x'^2/4)=\delta$. This relation is approximately valid only if

$$\delta\approx\beta\gg\frac{\nu^2x'^2}{4}. \tag{29}$$

Hence $\vartheta(x',\tau')$ will not involve higher modes and will be a stationary ground state only if Eq. (29) is valid at all points inside the box. Then it must also hold at $x'=1$. Thus $\Psi_0^2\approx\beta\gg\nu^2/4$—i.e., $\Psi_0\gg\nu/2$. If this is the case, then $\nu^2x'^2/4<\nu^2/4\ll\Psi_0^2\approx\beta$; hence, the relation $\beta+(\nu^2x'^2/4)=\delta$ appearing above reduces simply to $\beta\approx\delta$.

Consequently, if $2\Psi_0\gg\nu$, the ground states of Eq. (3) for $t<0$ and of Eq. (25) for $t>0$ coincide, implying that the full solution is simply $\vartheta(x',\tau')=\zeta(x')e^{-i\beta\tau'}$ and that $|\vartheta(0,\tau')|=1$. We note that $\zeta(x')$ has negative curvature right up to the wall, as is indeed expected in the case $2\Psi_0\gg\nu$, as we have already explained earlier.

Let us illustrate this result in the case of $\nu=15$, a value that would belong to the regime of the sudden approximation if Ψ_0 were zero. The solid curve in Fig. 9 represents the numerically obtained solution $\zeta(x')$ of Eq. (3), with Ψ_0

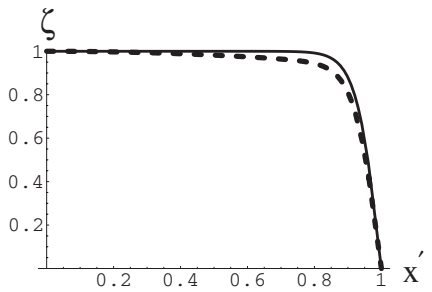

FIG. 9. The solid curve represents the numerically obtained solution $\zeta(x')$ of Eq. (3), with $\beta=400$ and $\Psi_0=19.99999999971558$, while the dashed curve represents the numerically obtained solution $\theta(x')$ of Eq. (25) for $\Psi_0=19.99999999971558$, $\nu=15$, and $\delta=400.2815489$. The two curves almost coincide, the ratio $2\Psi_0/\nu$ being 2.66.

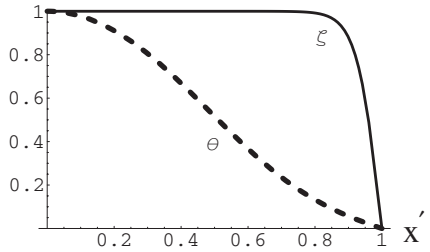

FIG. 10. The solid curve represents the numerically obtained solution $\zeta(x')$ of Eq. (3), with $\beta=16$ and $\Psi_0=3.78441$, while the dashed curve represents the numerically obtained solution $\theta(x')$ of Eq. (25) for $\Psi_0=3.78441$, $\nu=15$, $2\Psi_0/\nu=0.5046$, and $\delta=23.32954$.

≈ 20 and $\beta=400$, while the dashed curve represents the numerically obtained solution $\theta(x')$ of Eq. (25) for $\Psi_0 \approx 20$, $\nu=15$, $2\Psi_0/\nu=2.66$, and $\delta=400.281\,548\,9$. The numerical solution for $\zeta(x')$ was obtained by using the explicit Runge-Kutta method, the value of Ψ_0 having been found iteratively so as to satisfy $\zeta(1)=0$, while the numerical solution for $\theta(x')$ was obtained by using the explicit Runge-Kutta method for the very same value of Ψ_0, the value of δ having been found iteratively so as to satisfy $\theta(1)=0$. We see that these curves are quite close to each other, even though the ratio $2\Psi_0/\nu \approx 2.66$ is not too large.

In contrast, the numerically obtained solution $\zeta(x')$ of Eq. (3), with $\beta=16$ and $\Psi_0=3.784\,41$, represented by the solid curve in Fig. 10, does not coincide at all with the numerically obtained solution $\theta(x')$ of Eq. (25) for $\Psi_0=3.784\,41$, $\nu=15$, $2\Psi_0/\nu=0.5046$, and $\delta=23.329\,54$, represented by the dashed curve in the same figure.

The crucial role of the parameter $2\Psi_0/\nu$ is thus illustrated most clearly.

We can verify this result analytically by using the piecewise linearization of the cubic term in Eq. (25). If we perform a piecewise linearization of this cubic term, we obtain

$$\frac{d^2\theta}{dx'^2}+\frac{1}{x'}\frac{d\theta}{dx'}-\frac{\nu^2x'^2}{4}\theta+\delta\theta=\Psi_0^2(a\theta+b) \tag{30}$$

if $\zeta_0 \leqslant \theta \leqslant 1$ and

$$\frac{d^2\theta}{dx'^2}+\frac{1}{x'}\frac{d\theta}{dx'}-\frac{\nu^2x'^2}{4}\theta+\delta\theta=c\Psi_0^2\theta \tag{31}$$

if $0 \leqslant \theta \leqslant \zeta_0$.

Let us assume now that $\theta(R)=\zeta_0$. Let the solution be $\theta_{in}(x')$ for $0 \leqslant x' \leqslant R$, satisfying Eq. (30), and $\theta_{out}(x')$ for $R \leqslant x' \leqslant 1$, satisfying Eq. (31).

We can find an approximate partial solution to the inhomogeneous linear differential Eq. (30). Indeed, let us define the new variable

$$s=\frac{1}{a\Psi_0^2-\delta+\nu^2x'^2/4}. \tag{32}$$

For large Ψ_0 the variable s is small. Then, if we rewrite Eq. (30) in terms of s we can see that a partial solution is

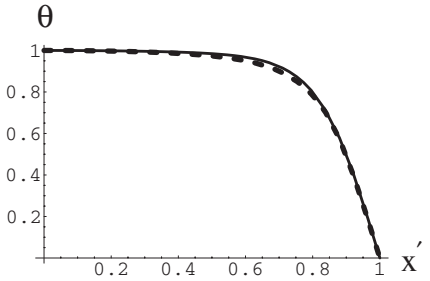

FIG. 11. The numerically obtained solution of Eq. (25) for $\Psi_0=8.9994907$, $\nu=5$, and $\delta=81.155759$, given by the solid line, and the analytic simulacrum of Eqs. (34) and (35) for the model values $\Psi_0=8.9994907$, $\nu=5$, $\delta=80.7789$, $R=0.869837$, $c_1=-0.539477$, and $c_2=0.00580057$, given by the dashed line.

$$-b\Psi_0^2s-b\nu^2\Psi_0^2s^3. \tag{33}$$

The homogeneous part of Eq. (30) can be solved in terms of confluent hypergeometric M functions. We thus obtain the approximate result (for large Ψ_0)

$$\theta_{in}(x') \approx -b\Psi_0^2s-b\nu^2\Psi_0^2s^3 + e^{-\nu x'^2/4}M\left(\frac{1}{2}+\frac{a\Psi_0^2-\delta}{2\nu},1,\frac{\nu x'^2}{2}\right) \times\left(1+\frac{b\Psi_0^2}{a\Psi_0^2-\delta}+\frac{b\nu^2\Psi_0^2}{(a\Psi_0^2-\delta)^3}\right). \tag{34}$$

This expression satisfies the differential equation (30), as well as the condition $\theta_{in}(0)=1$. Note that it does not involve the confluent hypergeometric U function, since U becomes infinite at the origin.

Similarly, Eq. (31) can be solved in terms of confluent hypergeometric functions, yielding

$$\theta_{out}=c_1e^{-\nu x'^2/4}M\left(\frac{1}{2}+\frac{c\Psi_0^2-\delta}{2\nu},1,\frac{\nu x'^2}{2}\right) + c_2e^{-\nu x'^2/4}U\left(\frac{1}{2}+\frac{c\Psi_0^2-\delta}{2\nu},1,\frac{\nu x'^2}{2}\right). \tag{35}$$

The unknown parameters are R, c_1, c_2, and δ. These parameters will be determined by the conditions

$$\theta_{out}(1)=0,$$

$$\theta_{in}(R)=\zeta_0,$$

$$\theta_{out}(R)=\zeta_0,$$

$$\frac{d\theta_{in}(R)}{dx'}=\frac{d\theta_{out}(R)}{dx'}. \tag{36}$$

When these conditions are satisfied, expressions (34) and (35) yield a very good emulation of the ground-state solution of Eq. (25), as shown in Fig. 11, where the numerically obtained solution of Eq. (25) for $\Psi_0=8.999\,490\,7$, $\nu=5$, and $\delta=81.155\,759$, given by the solid line, coincides almost perfectly with the simulacrum given by the dashed line for the

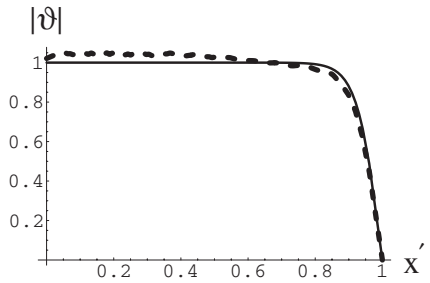

FIG. 12. The numerical solutions for the wave function $|\vartheta(x',\tau')|$ for $\beta=400$, $\Psi_0=19.99999999971558$, $\nu=17$, and $2\Psi_0/\nu=2.35$ for times $\tau'=0$ and $\tau'=\pi/(2\nu)$. The solid curve corresponds to the time $\tau'=0$, while the dashed curve corresponds to the time $\tau'=\pi/(2\nu)$.

model values $\Psi_0=8.999\,4907$, $\nu=5$, $\delta=80.7789$, $R=0.869\,837$, $c_1=-0.539\,477$, and $c_2=0.005\,800\,57$. This piecewise linearization is quite reliable for any values of Ψ_0 and ν.

Let us show now that the analytic simulacra of Eqs. (3) and (25) coincide when $2\Psi_0/\nu \gg 1$ and $\Psi_0 \gg 1$, by showing that the solutions of Eqs. (5) and (6) coincide with the solutions of Eqs. (30) and (31), even though ν may be large.

Since $\Psi_0 \gg 1$, we can drop the s^3 terms in Eq. (34), which then simplifies to

$$\theta_{in}(x') \approx -b\Psi_0^2 s + e^{-\nu x'^2/4} M\left(\frac{1}{2} + \frac{a\Psi_0^2 - \delta}{2\nu}, 1, \frac{\nu x'^2}{2}\right)\frac{\Psi_0^2 - \delta}{a\Psi_0^2 - \delta}. \tag{37}$$

However, for large a, $M(a,1,z) \approx e^{z/2} J_0(\sqrt{2z-4az})$ [13]. Hence this equation reduces to

$$\theta_{in}(x') \approx -b\Psi_0^2 s + I_0(x'\sqrt{a\Psi_0^2 - \delta})\frac{\Psi_0^2 - \delta}{a\Psi_0^2 - \delta}. \tag{38}$$

Furthermore, for large a we have $U(a,1,z) \approx \Gamma(1-a)e^{z/2}[\cos(\pi a)J_0(\sqrt{2z-4az}) - \sin(\pi a)Y_0(\sqrt{2z-4az})]$ [13]. Consequently Eq. (35) reduces to a linear combination of $J_0(x'\sqrt{\delta - c\Psi_0^2})$ and $Y_0(x'\sqrt{\delta - c\Psi_0^2})$. Then the requirements $\theta_{out}(R)=\zeta_0$ and $\theta_{out}(1)=0$ yield

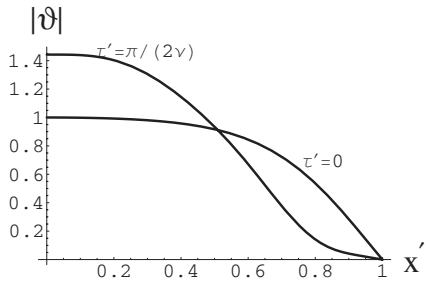

FIG. 13. The numerical solutions for the wave function $|\vartheta(x',\tau')|$ for $\beta=25$, $\Psi_0=4.93315$, $\nu=17$, and $2\Psi_0/\nu=0.58$ for times $\tau'=0$ and $\tau'=\pi/(2\nu)$.

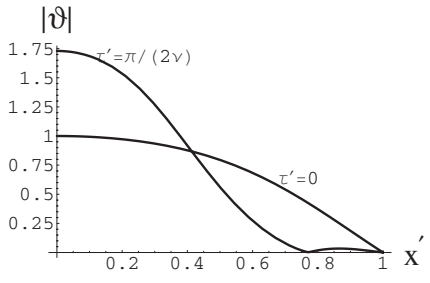

FIG. 14. The numerical solutions for the wave function $|\vartheta(x',\tau')|$ for $\nu=17$, $\beta=12$, $\Psi_0=3.05785$, and $2\Psi_0/\nu=0.36$ for times $\tau'=0$ and $\tau'=\pi/(2\nu)$.

$$\theta_{out}(x') \approx \zeta_0 \frac{J_0(x'\epsilon)Y_0(\epsilon) - J_0(\epsilon)Y_0(x'\epsilon)}{J_0(R\epsilon)Y_0(\epsilon) - J_0(\epsilon)Y_0(R\epsilon)}, \tag{39}$$

where $\epsilon=\sqrt{\delta - c\Psi_0^2}$.

The fact that $\theta_{in}(R)=\zeta_0$, even though for large Ψ_0 the Bessel function I_0 in Eq. (38) becomes huge, can only imply that $\delta \approx \Psi_0^2$. Therefore $\epsilon=\sqrt{\delta - c\Psi_0^2} \approx \Psi_0\sqrt{1-c} \approx k$. Furthermore, Eq. (39) yields $\theta'_{out}(R) \approx -\epsilon\zeta_0 \cot(\epsilon - R\epsilon)$ and

$$\theta_{out}(x') \approx \zeta_0 \sqrt{\frac{R}{x'}}\frac{\sin[\epsilon(1-x')]}{\sin[\epsilon(1-R)]}. \tag{40}$$

We note that the $\theta_{out}(x')$ of Eq. (40) has always got an inflection point at $1-x' \approx 4/(1+4\epsilon^2)$, for large Ψ_0. This inflection point is right on the wall, as seen already in Fig. 8.

As for the inner region, the use of Eq. (38) at the point $x'=R$ gives

$$\zeta_0 \approx \frac{-b\Psi_0^2}{a\Psi_0^2 - \delta + \nu^2 R^2/4} + I_0(R\sqrt{a\Psi_0^2 - \delta})\frac{\Psi_0^2 - \delta}{a\Psi_0^2 - \delta}. \tag{41}$$

However, we are examining the case $2\Psi_0 \gg \nu$. Hence Eq. (41) becomes

$$\frac{\zeta_0 - 1}{I_0(R\sqrt{a\Psi_0^2 - \Psi_0^2})} \approx \frac{\Psi_0^2 - \delta}{a\Psi_0^2 - \delta}. \tag{42}$$

Given that $2\Psi_0 \gg \nu$, we note now that the combination of Eqs. (42) and (38) yields the expression

$$\theta_{in}(x') \approx 1 + I_0(x'\sqrt{-b\Psi_0^2})\frac{\zeta_0 - 1}{I_0(R\sqrt{-b\Psi_0^2})}. \tag{43}$$

This expression yields $\theta'_{in}(R) \approx \Psi_0\sqrt{-b}(\zeta_0 - 1)$. Then the continuity of the slope of θ at R requires

$$\Psi_0\sqrt{-b}(1-\zeta_0) = \epsilon\zeta_0 \cot(\epsilon - R\epsilon). \tag{44}$$

The solution of this equation is $R=x_0$, where x_0 is given in Eq. (13). Consequently Eq. (39) yields a θ_{out} identical to the ζ_{out} of Eq. (11), since $R=x_0$. So ζ and θ are identical in the outer region, when Ψ_0 is large.

We also note that Eq. (7) reduces to

$$\zeta_{in}(x') \approx I_0(qx')\frac{\zeta_0 - 1}{I_0(qx_0)} + 1 \tag{45}$$

when Ψ_0 is large, with $q^2 \approx -b\Psi_0^2$. We see thus from Eqs. (45) and (43) that ζ_{in} and θ_{in} are indeed identical, with $R = x_0$, as long as Ψ_0 is large and $2\Psi_0 \gg \nu$. Therefore the profile $\zeta(x')$ of the wave function at $t=0$ coincides with the stationary ground state of Eq. (25) at $t>0$, provided $\Psi_0 \gg 1$ and $2\Psi_0 \gg \nu$.

We have thus a very interesting dependence of the behavior of the condensate in the rapidly expanding box on two parameters Ψ_0 and ν. In the linear region, where only ν counts, small values of ν correspond to the adiabatic approximation, while large values of ν correspond to the sudden approximation. Thus, for a rapidly expanding box with small nonlinearity the condensate does not keep up with the expanding box and an increasing void is created between the condensate and the wall of the box. The situation changes dramatically though when the nonlinearity is substantial, with $2\Psi_0 \gg \nu$. Then, even though the box is expanding rapidly, the condensate follows faithfully the moving wall and spreads uniformly over all of the box. We note that for a slowly expanding box the condensate always spreads uniformly over the whole area, since it does so in the linear case and the repulsion of the atoms can only strengthen the effect.

Let us now verify our analytic results numerically. In the region $2\Psi_0 > \nu$ the wave function spreads all over the box, with negative curvature, and it always remains in the ground state, with $|\vartheta(0,\tau')| = 1$, as shown in Fig. 12 for the particular case of $\beta = 400$, $\Psi_0 \approx 20$, $\nu = 17$, and $2\Psi_0/\nu = 2.35$.

As the ratio $2\Psi_0/\nu$ decreases, the condensate covers still the whole area, but with positive curvature, as shown in Fig. 13 for the particular case of $\beta = 25$, $\Psi_0 = 4.933\,15$, $\nu = 17$, and $2\Psi_0/\nu = 0.58$.

Finally, in the region $2\Psi_0 \ll \nu$ the condensate has retreated to the center of the box and a void has appeared between the wall and the condensate's boundary, as shown in Fig. 14 for the case of $\nu = 17$, $\beta = 12$, $\Psi_0 = 3.057\,85$, and $2\Psi_0/\nu = 0.36$. This numerical analysis confirms thus that the parameter $2\Psi_0/\nu$ determines whether the wave function will have to extend all the way up to the wall or not.

[1] T. P. Meyrath, F. Schreck, J. L. Hanssen, C.-S. Chuu, and M. G. Raizen, Phys. Rev. A **71**, 041604(R) (2005).

[2] Dario Poletti, Libin Fu, Jie Liu, and Baowen Li, Phys. Rev. E **73**, 056203 (2006).

[3] L. D. Carr, Charles W. Clark, and W. P. Reinhardt, Phys. Rev. A **62**, 063610 (2000); **62**, 063611 (2000).

[4] Y. B. Band, Boris Malomed, and Marek Trippenbach, Phys. Rev. A **65**, 033607 (2002).

[5] V. V. Dodonov, A. B. Klimov, and D. E. Nikonov, J. Math. Phys. **34**, 3391 (1993); S. V. Melnichuk, W. van Dijk, and Y. Nogami, Eur. J. Phys. **26**, 121 (2005).

[6] M. V. Berry and G. Klein, J. Phys. A **17**, 1805 (1984); A. J. Makowski and S. T. Dembinski, Phys. Lett. A **154**, 217 (1991).

[7] S. Theodorakis, Phys. Rev. E **67**, 066701 (2003).

[8] Stavros Theodorakis and Yiannis Constantinou, Phys. Lett. A **364**, 497 (2007).

[9] A. Munier, J. R. Burgan, M. Feix, and E. Fijalkow, J. Math. Phys. **22**, 1219 (1981); J. R. Burgan, M. R. Feix, E. Fijalkow, and A. Munier, Phys. Lett. **74A**, 11 (1979).

[10] S. T. Dembinski and L. Wolniewicz, J. Phys. A **29**, 349 (1996).

[11] Alberto Devoto and Bojan Pomorisac, J. Phys. A **25**, 241 (1992); S. W. Doescher and M. H. Rice, Am. J. Phys. **37**, 1246 (1969); D. N. Pinder, *ibid.* **58**, 54 (1990).

[12] Y. B. Band and Marek Trippenbach, Phys. Rev. A **65**, 053602 (2002).

[13] *Handbook of Mathematical Functions*, edited by Milton Abramowitz and Irene A. Stegun (Dover, New York, 1970), p. 508.